Silicon Encapsulated Carbon Nanotubes

**Sri Lakshmi Katar · Azlin Biaggi Labiosa ·
Amairy E. Plaud · Edgar Mosquera-Vargas ·
Luis Fonseca · Brad R. Weiner · Gerardo Morell**

Abstract A dual stage process of depositing bamboo-like carbon nanotubes (BCNTs) by hot filament chemical vapor deposition (HFCVD) and coating Si using Radio frequency sputtering (RFS) technique. The films were characterized by scanning electron microscopy (SEM), transmission electron microscopy (TEM), Raman spectroscopy, X-ray photo-electron spectroscopy (XPS), and electron field emission studies (EFE). SEM results suggest a dense network of homogeneous silicon-coated BCNTs. From the comprehensive analysis of the results provided by these techniques emerges the picture of Si encapsulated BCNTs.

Keywords BCNTs · Silicon coated · Sputtering

S. L. Katar · E. Mosquera-Vargas · L. Fonseca ·
B. R. Weiner · G. Morell
Institute for Functional Nanomaterials, University of Puerto Rico, San Juan, PR, USA

S. L. Katar (✉) · A. E. Plaud · B. R. Weiner
Department of Chemistry, University of Puerto Rico,
P.O. Box 23323, San Juan, PR 00931, USA
e-mail: srilakshmikatar@yahoo.com

E. Mosquera-Vargas · L. Fonseca · G. Morell
Department of Physics, University of Puerto Rico,
P.O. Box 23343, San Juan, PR 00931, USA

A. B. Labiosa
Sensors and Electronics Branch, Instrumentation and Controls Division, National Aeronautics and Space Administration Glenn Research Center, 21000 Brookpark Road, Cleveland, OH 44135, USA

Introduction

Silicon is an important material due to its role as the fundamental component in integrated circuits, microelectronics, and in lithium ion batteries. Continuous efforts have been focused on investigating the nanostructures of silicon for unveiling the properties and miniaturizing the microelectronics devices, including the goal of integrating the electronics and photonics on the same Si chip. To attain this challenge various groups reported silicon nanotubes, each using a different growth process. Yang et al. [1, 2] first reported the synthesis by chemical vapor deposition and experimental observation by transmission electron microscopy (TEM) of large-diameter SiNTs. The tubes were grown on alumina nanochannel arrays using gold particles as catalysts. Lee and co-workers [3] later reported the growth of SiNTs by molecular beam epitaxy on porous alumina, without using catalysts. The observed tubular structures were covered with a thick layer of silicon oxide. Sol–gel methods have resulted in SiO_x-coated MWCNTs. A drawback of this technique was that the sintering process led to a partial crystallization of the SiO_2 resulting in a very inhomogeneous matrix [4]. An alternative method, which avoids these problems, has been developed. This involves using a Nd:YAG laser to rapidly heat a tetraethoxysilane/nanotube mixture, resulting in partial melting of the matrix. This produced an amorphous silica matrix, with no crystallization. A novel nanotube/silica composite material with potentially useful optical properties has recently been described by Han et al. [5]. These workers synthesized films consisting of silica spheres with diameters ranging from 200 to 650 nm. Molybdenum/cobalt catalyst particles were then deposited onto the silica spheres and used to catalyze the growth of SWNTs. Since SWNTs are highly non-linear and fast-switching materials, they can be incorporated into an

optically confining environment to achieve these characteristics at relatively low levels of laser intensities. There have also been some initial studies on carbon nanotube/carbon fibre composites [6]. Wang et al. [7] reported the thermal characteristics of silicon-coated multiwalled carbon nanotubes. In this article, we discuss the synthesis, and characterization of silicon-coated bamboo like carbon nanotubes (BCNTs) using HFCVD and RF sputtering for lithium ion rechargeable battery anodes. The novelty of this work is to be able to fabricate a nano Si composite anode material, which addresses the 400% volume expansion of Si electrodes. The electrochemical characterization results will be published as a separate article.

Experimental

The BCNT films deposited on copper substrates used in this study were grown in a custom made HFCVD chamber which has been previously described in detail elsewhere [8]. Tungsten wire (99.95% pure, 0.5 mm diameter) was wound as a helical spring filament in the HFCVD. Before the thin films deposition, the tungsten filament was carburized. For this, we pumped down the CVD chamber to 8×10^{-6} mbar (6.0×10^{-6} Torr) and then filled it with a mixture of 2.0% CH_4, 98.0% H_2 with 500 ppm of H_2S. Maintaining the combined flow of gases at 100 sccm, and a pressure of 20 Torr, we kept a constant current of 20 A through the tungsten wire for 8 h. Starting the carburization process, the voltage across the filament was 7.7 V, indicating a low resistance for pure tungsten, but as the time progressed, the voltage increased, reaching 17.0 V after 8 h.

Polycrystalline copper substrates (99.9% pure, 0.5 mm thick, 14 mm disk diameter) were hand polished with 600-grit sandpaper on both sides to make them flat. One side was then further polished with 1000, 1500, and 2000 grit sandpaper to smooth the surface. The last step of the polishing was made with diamond powder (<1 μm particle size) to achieve a mirror-like surface and for diamond scratching and seeding, to enhance the nucleation. Before the diamond powder polishing, the substrates had a natural copper color, and after the powder polishing, the substrates looked darker. The substrates were then cleaned in an ultra sonic bath with 2-propanol for 15 min, dried with helium, and inserted in the HFCVD chamber on top of a molybdenum substrate holder.

Prior to each deposition, we pumped down the CVD chamber to 8×10^{-6} mbar (6.0×10^{-6} Torr) and then introduced the gases. For all the samples discussed in this paper, we kept constant the gas mixture of 2.0% CH_4, 98% H_2 with 500 ppm of H_2S, the combined flow of the gases to 100 sccm, the deposition pressure at 20 Torr, the filament temperature at ~2500 °C, and the filament-substrate distance to 8 mm. The only parameters changed were the substrate temperature and the deposition time. We grew at 900 °C for 15 min. The deposition time was selected in order to achieve a film that covered the whole substrate that did not experience peeling or delamination from the copper substrate for the selected substrate temperature.

Experimental Setup for Sputtering of BCNTs

For deposition of the BCNTs with Si, the samples were placed on the vacuum chamber of a Varian RF sputtering machine. The samples were sputtered with a Si target for 30 min. The samples were placed on a substrate holder with carbon tape and the holder was then placed on the vacuum chamber. A silicon target is used. Before starting the deposition, the residual pressure inside the vacuum chamber was $\sim 2 \times 10^{-7}$ Torr. During the sputtering process the argon pressure was kept at 20 mTorr, while the target was at a voltage of 1050 V and with a forward power of 50 W.

Scanning electron microscopy using a JEOL model 35 CF microscope revealed the surface morphology. Raman spectroscopy is used to analyze the structure. The Raman spectra were recorded using a triple monochromator (ISA J-Y Model T64000) using the 514.5 nm line of Ar laser. The spectra were recorded using an 80× objective, and the probed area was of 1–2 μm^2. The power on the sample was kept below 10 mW to avoid damage. Silicon was used to calibrate the Raman peak position.

A JEOL 3010 high-resolution transmission electron microscope operating at 300 kV was used to observe the morphology and microstructure of the BCNTs samples. The morphological and microstructural analysis on the nanometer scale was carried out using a Carl Zeiss LEO 922 electron microscope operating at an accelerating voltage of 200 keV. The ESI elemental maps were calculated from the electron energy-loss images by the three-window technique described in the digital micrograph software. In this method, three images from the transmitted electrons filtered through three different energy regions with energy windows of predetermined width are collected sequentially using a CCD camera. Currently, EELS provides superior capability in identifying and quantifying light elements under nanometer scales. Copper grids from Ted Pella (Redding, CA) coated with a thin amorphous carbon were used for the Transmission Electron Microscopy (TEM) studies. The TEM samples were prepared by spreading onto the TEM grids a drop of ultrasonically dispersed materials in water, and allowing them to dry in air.

The X-ray photoelectron spectroscopy (XPS) analysis was carried out in the ultra-high vacuum (UHV) chamber (5×10^{-9} Torr) of a Physical Electronic 5600 X-ray photoelectron spectrometer. The Al X-ray monochromatic source was kept at a power of 350 W with 15 kV, and the pass energy used for the measurements was of 187.85 and 5.85 eV. The C 1s, O 1s, and Si 2p spectra were obtained for BCNTs coated with Si. The 933.00 eV Cu 2p peak was used to calibrate the spectral frequency whenever minor charging effects (less than 1 eV) were observed. The fitting of all spectra was done with mixed Gaussian Lorentzians, unless other wise stated, using the Casa XPS program.

Field Emission IV characteristics were measured in a custom made system, described in detail elsewhere [9]. Briefly, a diode configuration is used, in which a molybdenum rod of 3 mm diameter (area: 0.071 cm^2) serves as the anode. Voltage is applied using a Stanford Research Systems PS350 power supply. The emitted current is measured with a Keithley 6517A electrometer. For the configuration employed, the macroscopic surface electric field (E_S) on the sample (i.e., cathode) can be estimated accurately by $E_S = V/d_{CA}$, where V is the voltage applied to the anode and d_{CA} is the distance between the anode and the cathode [10]. All the measurements were taken at $d_{CA} = 100 \pm 2$ μm, and at a pressure of $1-2 \times 10^{-7}$ Torr ($1.3-2.7 \times 10^{-7}$ mbar). Currents lower than 1×10^{-12} A was considered at the background noise level. The current density was calculated by dividing the current over the area of the sample subjected to $E_S = V/d_{CA}$, which, in our specific configuration, is well-approximated by using the area of the anode (0.071 cm^2) [10]. The turn-on field (E_t) was defined as the electric field necessary to emit a current density of 10 μA/cm^2 [11]. Each data point in the I–V curves is the average of 8 measurements taken 250 ms apart. For data acquisition, a custom Lab View (National Instruments) program was developed. As a measure of precaution to avoid the influence of displacement or charging current in the field-emitted current, specifically in currents smaller than 1×10^{-11} A, a delay of 4 s between the change in voltage and the data acquisition was employed.

Results and Discussions

The SEM images in the Fig. 1a, b shows the uncoated bamboo like carbon nanotubes deposited by HFCVD. Figure 1c, d shows the silicon-coated BCNTs with increase in the diameter and surface roughness upon sputtering. To learn more about the structure of these BCNTs, we conducted TEM measurements. Figure 2a and b are the TEM images of the silicon-coated BCNTs revealing a diameter of $\sim$80–100 nm. The inner nanocavities of the BCNTs are not clearly seen may be due to the intense coverage of silicon allover the nanotubes. The elemental mapping results (Fig. 3) suggest that silicon and carbon are equally distributed in the sample and both have identical mappings. The O (Fig. 3b) map shows a uniform distribution on the tube and the grid consistent with a contaminant species.

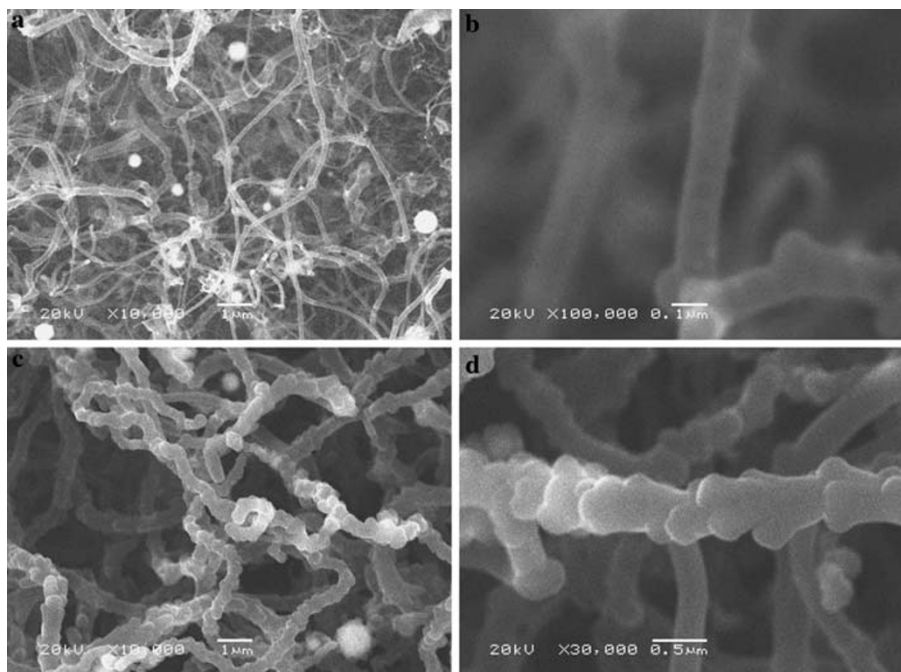**Fig. 1** SEM micrographs of the **a**, **b** BCNTs and **c**, **d** Si-coated BCNTs

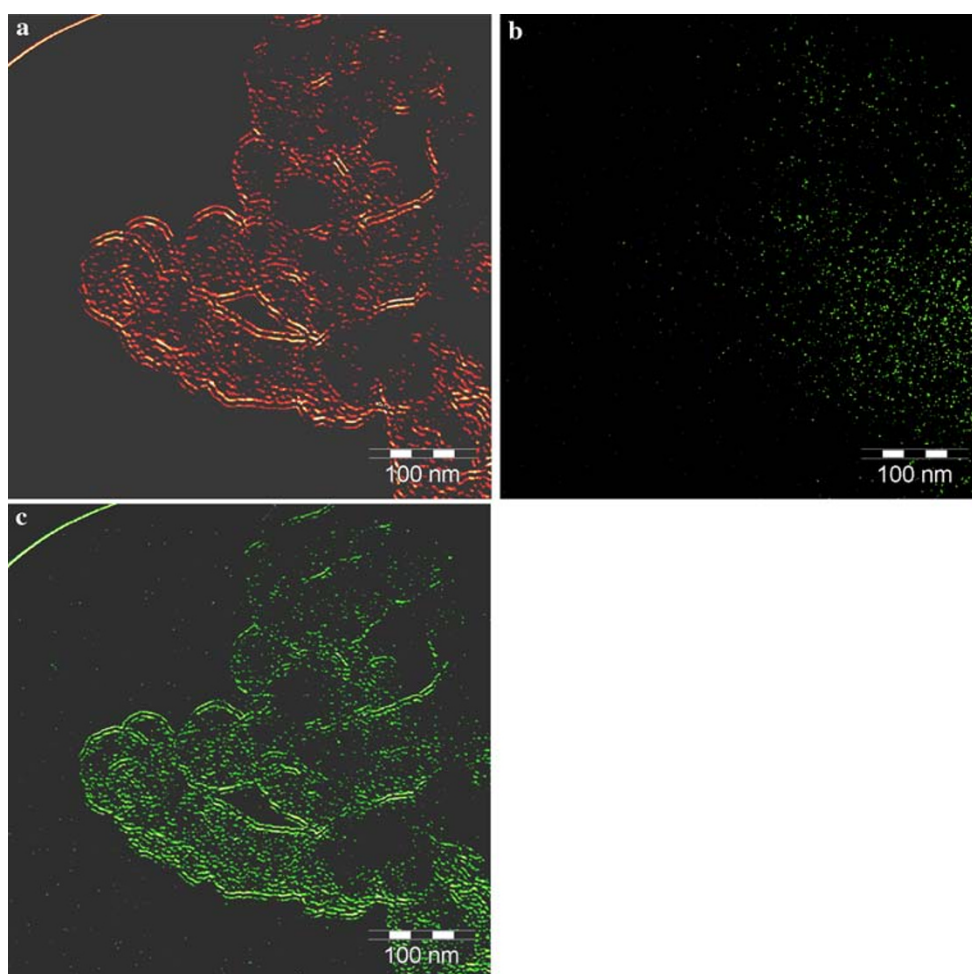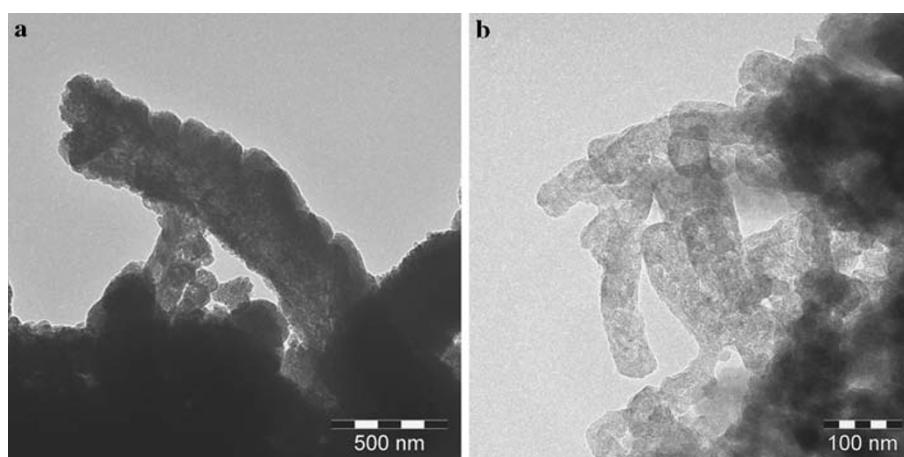**Fig. 2** TEM images of the Si-coated BCNTs

Fig. 3 Elemental mapping of the Si-coated BCNTs: **a** carbon, **b** oxygen, **c** silicon

Raman Spectroscopy

Figure 4 shows the Raman spectra of Si-coated BCNTs and silicon film on copper substrates. The intense peak at around 500 cm^{-1} is ascribed to the transverse optical phonon modes of crystalline silicon [12]. The red shift of this peak with respect to bulk Si crystals (521 cm^{-1}) can be attributed to confinement effects [13, 14]. The broad bands in the 250–350 and 900–1000 cm^{-1} regions correspond to the acoustic modes and the second order Raman signal of
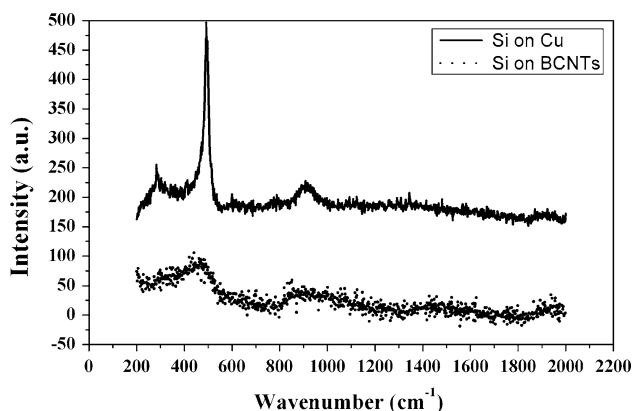
Fig. 4 Raman spectra of (a) Si on Cu (b) Si-coated BCNTs

silicon, respectively. Both of them became enhanced by small crystallite size effects. When Si is deposited on BCNTs, all the transverse optical phonons in the Brillouin become activated due to the reduced phonon coherence length, thus producing a very broad band in the 350–550 cm^{-1} region, consistent with the formation of nano-SiC [15]. Similarly, the broad band in the 800–1100 cm^{-1} region confirms the formation of nano-SiC on the BCNTs. Furthermore, the absence of C bands in the 1350 and 1600 cm^{-1} regions indicates that the nano-SiC coating is very uniform, completely masking the underlying BCNTs. The Raman excitation energy employed (2.5 eV) is completely absorbed within the thickness of the nano-SiC coating.

X-ray Photo Electron Spectroscopy

Figure 5 shows the XPS regions of Si 2p, C 1s, and O 1s for the BCNTs sputtered for 30 min (upper row) and 1 h (lower row). The broad and asymmetrical Si 2p peak indicates that the chemical state of the Si element is not single. It was resolved into three peaks. The first two peaks at ~100.5 and ~101.0 eV are the Si doublet, as expected. The third peak at ~102.7 eV is associated to SiC, thus confirming its presence in agreement with the characterizations discussed above. The C 1s band can be resolved into two peaks, one centered at ~283.0 eV, which is associated to silicon carbides, and another at ~284.0 eV, which is assigned to graphitic carbon. The O 1s band is centered at ~532.2 eV and can resolved into two peaks: one at ~532.1 eV, associated to carbonates, and another at ~532.9 eV, associated to SiO$_2$.

Field Emission Results

The field emission properties can be affected by the band gap, electron affinity, interfacial quality, and microstructural morphology [16, 17]. These Si-coated BCNTs
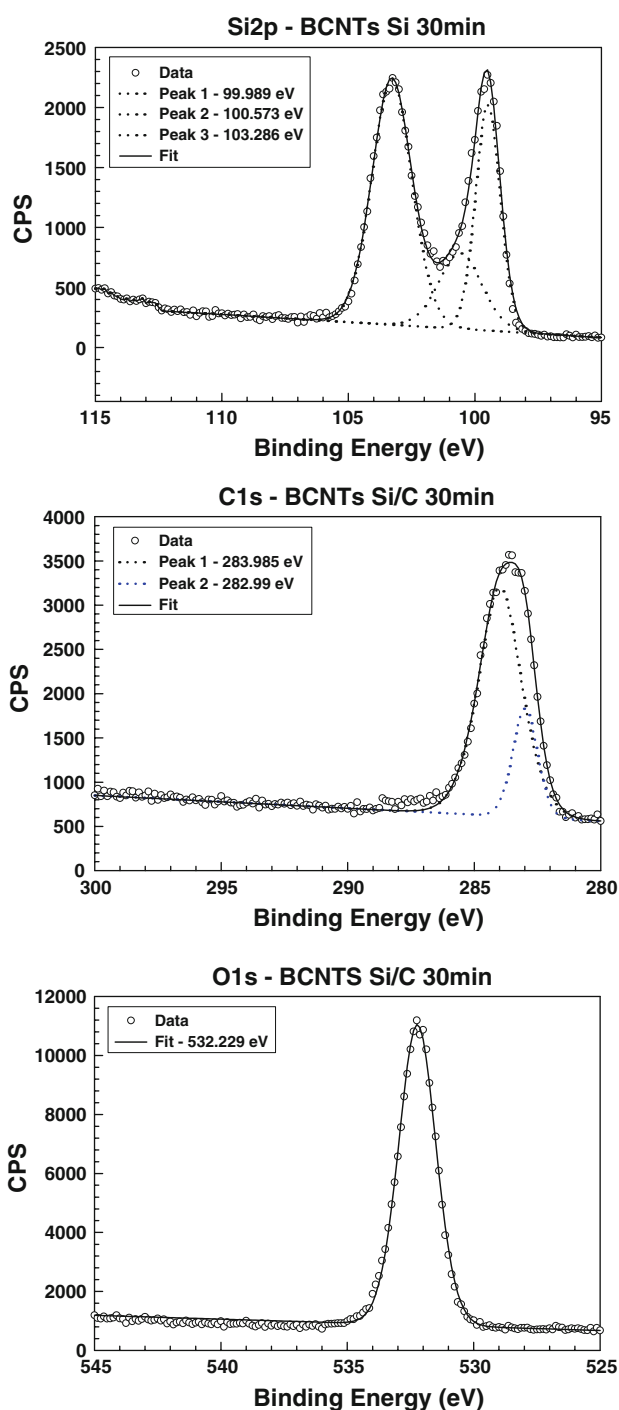

Fig. 5 XPS spectra of Si-coated BCNTs corresponding to Si 2p, C 1s, and O 1s

(Fig. 6) show field emission properties that indicate the existence of a good electrical interface between the substrate and the BCNTs, which formed by direct deposition (i.e., no catalyst or buffer layer), and between the Si coating and the BCNTs. The turn-on field changed from 3.1 eV for BCNTs to 4.7 eV for Si-coated BCNTs, which is consistent with the formation of a thin Si layer and an
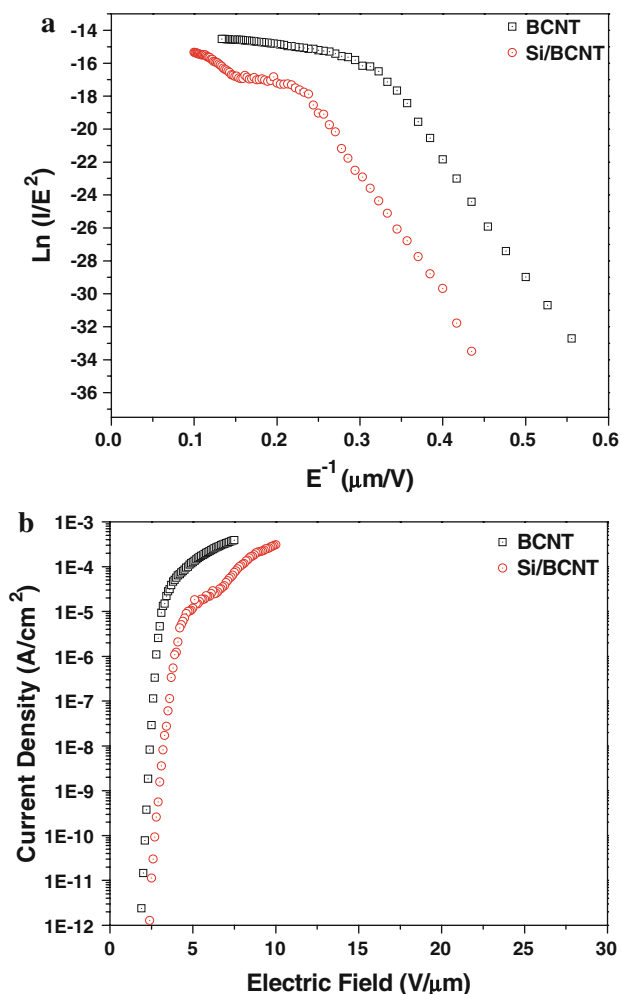
Fig. 6 Field emission response of Si-coated BCNTs and BCNTs **a** I–V curves, **b** F–N curves

as electrochemical active materials, though the present coating is in a multi-phase state, such as silicon, silicon carbide, silicon oxides are present in the sample. Due to the insulating properties of SiO_2 it does not contribute to the overall capacity were as Silicon carbide and silicon. The electrochemical properties of these individual phases add up to the total capacity of the electrochemical cell. But we expect the Si/BCNT material to exhibit properties similar to a silicon nanocomposite material. The BCNTs were successfully coated with a thin layer of Si. The Si/BCNT material has a diameter of ~ 80–100 nm. The elemental mapping indicates that Si is distributed uniformly over the BCNTs. Raman spectroscopy confirmed that the Si coating formed a homogeneous nano-SiC layer and XPS indicates the presence of C–Si and Si–O bonds, which are consistent with the Si encapsulation of BCNTs. Field emission results confirm that the Si layer is in excellent contact with the BCNTs and indicate that the Si nano layer can be employed as a protective layer in BCNTs field emission devices.

amorphous SiC interlayer. For comparison, the turn-on field previously reported for uncoated BCNTs is around 3 V/μm [11] and that of Si tips is around 5 V/μm [18]. The experimental results show an increase of the FN slope and of the turn-on field, which indicate that the effective work function of the coated structures increased and/or the enhancement factor decreased. The decrease on the enhancement factor is expected after the coating for two reasons: the increasing thickness of the tips and the modification of the local electric field due to the coating. The changes on the effective work function are related to different effects like the formation of an interfacial layer and surface states.

Conclusions

Various characterizations demonstrated the successful silicon coating on the CNTs, which is potentially useful

References

1. J. Sha, J. Niu, X. Ma, J. Xu, X. Zhang, Q. Yang, D. Yang, Adv. Mater. **14**, 1219 (2002)
2. O.G. Schmidt, K. Eberl, Nature **410**, 168 (2001)
3. S.Y. Jeong, J.Y. Kim, H.D. Yang, B.N. Yoon, S.H. Choi, H.K. Kang, C.W. Yang, Y.H. Lee, Adv. Mater. **15**, 1172 (2003)
4. T. Seeger, P. Redlich, N. Grobert, M. Terrones, D.R.M. Walton, H.W. Kroto, M. Ruhle, Chem. Phys. Lett. **339**, 41–46 (2001)
5. H. Han, S. Vijayalakshmi, A. Lan, Z. Iqbal, H. Grebel, E. Lalanne, A.M. Johnson, Appl. Phys. Lett. **82**, 1458–1460 (2003)
6. R. Andrews, D. Jacques, A.M. Rao, T. Rantell, F. Derbyshire, Y. Chen, J. Chen, R.C. Haddon, Appl. Phys. Lett. **75**, 1329–1331 (1999)
7. Y.H. Wang, Y.N. Li, J. Lu, J.B. Zang, H. Huang, Nanotechnology **17**, 3817–3821 (2006)
8. S. Gupta, B.L. Weiss, B.R. Weiner, G. Morell, Carbon films. J. Appl. Phys. **89**, 5671–5675 (2001)
9. G. Morell, A.G. Berrios, B.R. Weiner, S. Gupta, J. Mater. Sci. **17**, 443 (2006)
10. A.G. Berríos, F. Piazza, G. Morell, J. Vac. Sci. Technol. B **23**, 645 (2005)
11. S.L. Katar, A.G. Berríos, J.D. Jesus, B.R. Weiner, G. Morell, J. Nanomaterials **2008**, 7 (2008). doi:10.1155/2008/515890
12. H. Richter, Z.P. Wang, L. Ley, Solid State Commun. **39**, 625 (1981)
13. S.L. Zhang, Y. Hou, K.S. Ho, B. Qian, S. Cai, J. Appl. Phys. **72**, 4469 (1992)
14. P.V. Houng, P.H. Khoi, N.T.T. Tam, P.L.P. Hoa, L.T.C. Tuong, Int. J. Inorg. Mater. **1**, 209 (1999)

15. G. Morell, R.S. Katiyar, S.Z. Weisz, I. Balberg, J. Non Crystalline Solids **194**, 78 (1996)
16. B.S. Satyanarayana, X.L. Peng, G. Adamopoulos, J. Robertson, W.I. Milne, T.W. Clyne, Mat. Res. Soc. Symp. Proc. **621**, Q5.3.1–Q5.3.7 (2000)
17. D. He, L. Shao, W. Gong, E. Xie, K. Xu, G. Chen, Diamond Relat. Mater. **9**, 1600–1603 (2000)
18. C. Mu, Y.X. Yu, W. Liao, X.S. Zhao, D.S. Xu, X.H. Chen, D.P. Yu, Appl. Phys. Lett. **87**, 113104 (2005)